Journal of Alloys and Compounds 508 (2010) 251–257

Contents lists available at ScienceDirect

Journal of Alloys and Compounds

journal homepage: www.elsevier.com/locate/jallcom

High-pressure behavior of otavite ($CdCO_3$)

R. Minch[a,*], D.-H. Seoung[b], L. Ehm[c,d], B. Winkler[e], K. Knorr[f], L. Peters[a], L.A. Borkowski[c], J.B. Parise[g], Y. Lee[b], L. Dubrovinsky[h], W. Depmeier[a]

[a] Institut für Geowissenschaften, Christian-Albrechts-Universität zu Kiel, D-24118 Kiel, Germany
[b] Department of Earth System Science, Yonsei University, Seoul, Republic of Korea
[c] Mineral Physics Institute, Stony Brook University, Stony Brook, NY 11794, USA
[d] National Synchrotron Light Source, Brookhaven National Laboratory, Upton, NY 11973, USA
[e] Institut für Geowissenschaften, Abteilung für Kristallographie, Universität Frankfurt, D-60438 Frankfurt am Main, Germany
[f] BrukerAXS GmbH, 76187 Karlsruhe, Germany
[g] Department of Geosciences, Stony Brook University, Stony Brook, NY 11794, USA
[h] Bayerisches Geoinstitut, Universität Bayreuth, D-95447 Bayreuth, Germany

ARTICLE INFO

Article history:
Received 16 February 2010
Received in revised form 18 August 2010
Accepted 24 August 2010
Available online 25 September 2010

Keywords:
Inorganic materials
Crystal structure and equation-of-state
High-pressure
X-ray diffraction
Optical spectroscopy

ABSTRACT

The high-pressure, room temperature behavior of otavite ($CdCO_3$) was investigated by angle-dispersive synchrotron radiation powder diffraction up to 40 GPa, Raman spectroscopy up to 23 GPa and quantum mechanical calculations based on density functional theory. The calcite-type structure of $CdCO_3$ is stable up to at least ~19 GPa as shown by Raman spectroscopy. The compression mechanism was obtained from structure refinements against the diffraction data. The quantum mechanical calculations propose a calcite–aragonite phase transition to occur at about 30 GPa. The existence of a pressure-induced phase transition is supported by the Raman and diffraction experiments. Evidence for the transformation is given by broadening of X-ray reflections and external Raman bands starting from about 19 GPa in both experiments.

1. Introduction

Otavite, $CdCO_3$, is a representative of carbonates with calcite-type structure [1]. It is the principal natural resource for mining Cd, which finds its main application in the production of Ni–Cd batteries [2]. At ambient conditions, cadmium carbonate crystallizes in the trigonal space group *R*-3*c* with cell parameters $a = 4.923(3)$ Å, $c = 16.287(6)$ Å [3] in the hexagonal setting. The cadmium ions occupy Wyckoff position 2*b* (0, 0, 0) and are octahedrally coordinated by oxygen (Fig. 1). The CO_3 group is planar, with carbon occupying Wyckoff position 2*a* (0, 0, 1/4) and oxygen the 6*f* (x, 0, 1/4) position. Otavite is isostructural with calcium carbonate and the ionic radius of Cd^{2+} (0.95 Å) differs only slightly from that of Ca^{2+} (1.00 Å) [4]. Therefore, it may be expected, that otavite would have a high-pressure behavior similar to calcium carbonate. However, Cd^{2+} has a significantly different electron configuration than Ca^{2+}, which biases the high-pressure behavior of otavite.

Room temperature *in-situ* X-ray diffraction experiments in a multi-anvil cell were performed to determine the bulk modulus (B_0) of the complete set of calcite-type carbonates in the pressure range 0–8.1 GPa [5]. For otavite, values of $B_0 = 97(1)$ and 98(1) GPa were obtained in two experimental runs. Generally, the compressibility of the calcite-type carbonates was found to depend on the cation which mainly biases the character of compressibility along the *a*-axis. Compressibilities of the *a*-axis decrease in the following order: *s* element carbonates ($MgCO_3$, $CaCO_3$), 3*d* transition metal carbonates ($NiCO_3$, $MnCO_3$, $CoCO_3$, $FeCO_3$) and 4*d* transition metal carbonate ($CdCO_3$). No influence of the type of cation on the stability of the calcite structure type up to 8 GPa at ambient temperature was reported by Zhang and Reeder [5], since they did not observe phase transitions for the compounds investigated, except for calcite, which showed a phase transition to the calcite-II structure at 2 GPa.

A p_T-induced phase transition in $CdCO_3$ to an aragonite-type structure was reported by Liu and Lin [6] for samples quenched from 18 to 25 GPa and ≈1000 °C. From X-ray diffraction of the quenched sample, the lattice parameters of the proposed aragonite-type $CdCO_3$ were determined to be $a = 4.489(3)$ Å, $b = 7.822(3)$ Å, $c = 5.713(4)$ Å at ambient conditions.

The aim of this investigation was to show, using Cd^{2+}, that the complex electron configuration of *d* transition metals sets their high-pressure behavior apart from the pressure-homologous rule [7], according to which isostructural compounds containing dif-

* Corresponding author. Present address: Institute for Materials and Surface Technology, D-24149 Kiel, Germany, Tel.: +49 431 210 2625; fax: +49 431 210 2660.
E-mail address: robert.minch@fh-kiel.de (R. Minch).

0925-8388/$ – see front matter © 2010 Elsevier B.V. All rights reserved.
doi:10.1016/j.jallcom.2010.08.090

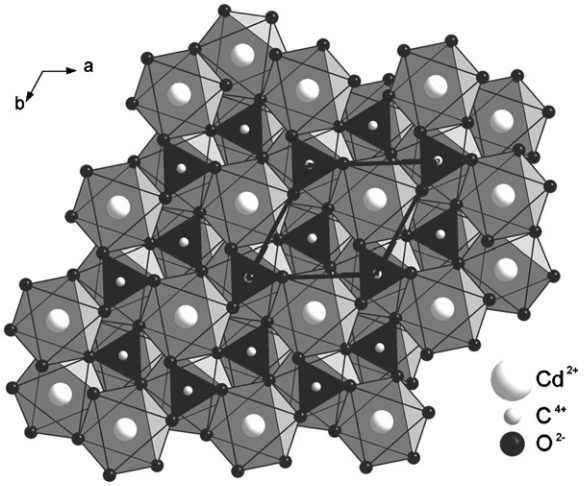

Fig. 1. Crystal structure of $CdCO_3$, projected along the *c*-axis. Cd atoms (big white spheres) are at the center of octahedra (light-gray), coordinated by oxygen (small black spheres). The CO_3 groups (black triangles with the C atom (small white sphere) at the center) are planar.

ferent cations undergo similar phase transitions but at different pressures. Additionally, we wanted to prove, whether otavite has the previously documented calcite–aragonite phase transition [6]. Such type of transition has not been published up to now for other *d* transition metal carbonates with calcite structure at ambient conditions. It was demonstrated for $FeCO_3$ and $MnCO_3$ that the calcite structure is stable for each of those carbonates up to 50 GPa at 300 K and up to 47 GPa with heating to 2000 K [8]. Recently, Ono [9] found a phase transition in $MnCO_3$ from calcite-type to a new high-pressure polymorph. The diffraction pattern could be indexed with an orthorhombic unit cell, however, the cell parameters of the new cell are inconsistent with those of an aragonite-type structure.

The increasing availability of *in-situ* high-pressure facilities stimulated the unimpaired interest in systematic work on carbonates during the past few years [10–14]. As part of our comprehensive investigation of the crystal chemistry of carbonates [15–16], we have studied the high-pressure behavior of $CdCO_3$ *in situ*. Herein, we present results obtained from synchrotron powder diffraction up to 40 GPa, Raman spectroscopy up to 23 GPa and density functional theory (DFT) calculations.

2. Experimental methods

2.1. High-pressure powder diffraction

Commercial, extra pure $CdCO_3$ was used for the experiments (99.999%, Alfa Aesar). High-pressure X-ray powder diffraction experiments up to 40 GPa were carried out at beamline X17C at the National Synchrotron Light Source (Brookhaven National Lab., USA) using the *in situ* high-pressure angle-dispersive X-ray diffraction system and a standard diamond anvil cell. The beamline optics consisted of a Si (3 3 1) double-crystal monochromator and Kirkpatrick/Baez mirrors which provide a beam size at the sample of $25 \times 30\ \mu m^2$. High-pressure patterns up to ~40 GPa were collected at a wavelength of 0.4066 Å using a MAR165 CCD detector. The exposure time per image was about 40 min.

Diamonds with 300 μm culet size were used. A Rhenium gasket was pre-indented to a thickness of about 40 μm with a sample chamber of 100 μm diameter. The sample and a number of ruby chips for pressure calibration were loaded into the sample chamber. The Mao pressure scale was applied for pressure determination by the ruby fluorescence method [17]. Neon was used as the pressure transmitting medium.

Geometry parameters for the radial integration of the two-dimensional diffraction data were determined from a CeO_2 [18] sample. The two-dimensional diffraction patterns were integrated and transformed into standard one-dimensional powder patterns using the software *FIT2D* [19]. The Rietveld method [20] within the *TOPAS* suite of programs [21] was used to determine lattice and structural parameters. The background was described by a tenth order polynomial and the peak profiles were modelled with a pseudo-Voigt function [22].

The preferred orientation of the gasket material Rhenium was accounted for by using the March-Dollase correction [23]. Lattice parameters of $CdCO_3$ and the *x*-coordinate of the oxygen atom were the refinable structural parameters. Structure refinements were performed with the parameters unconstrained with an exception of the geometry of the carbonate group that was constrained using a C–O bond length of 1.28(1) Å and O–C–O angles 120(1)°. Because of the well-known fact of systematically too small *e.s.d.*'s from Rietveld refinements, errors for the refined unit cell were corrected by an estimated SCOR value of 3 [24]. All χ^2 values from the Rietveld refinement are around 1. The unit cell volume V_0 at a pressure of 0 GPa, the bulk modulus B_0 and its pressure derivative B_0' were determined from fits of a third-order Birch–Murnaghan equation-of-state to the measured cell volumes [25].

2.2. High-pressure spectroscopy

Raman spectra in the wave number range 150–1800 cm^{-1} were collected using a DILOR spectrometer with a 514.5 nm Ar^+ ion laser as the excitation light source. The scattered light was collected in backscattering geometry using a liquid nitrogen cooled CCD detector with a resolution of ±2 cm^{-1}. The ambient pressure spectrum of otavite was measured using standard Raman spectroscopy technique without using a DAC. The high-pressure Raman spectra were obtained using a BGI-type DAC [26], a 25× microscope objective, and three accumulations with 600 s integration time.

Ultra-low fluorescence 16-sided type Ia diamonds with 300 μm culet size were used. The pressure was determined by the ruby fluorescence method following the Mao pressure scale [17] with Neon as the pressure transmitting medium. A Rhenium gasket was pre-indented and a hole with a diameter of 150 μm was drilled at the center that served as sample chamber. Both, the Raman spectra and the ruby fluorescence, were measured from the same illuminated area in the cell. The pressure uncertainty is estimated to be 0.1 GPa. The positions of the Raman peaks and their full width at half maximum were determined by fitting Lorentzian functions using the *OPUS* v5.5 software (Bruker, 2004).

2.3. Computational details

The quantum mechanical calculations described here are based on density functional theory (DFT). The Perdew–Burke–Ernzerhof-version of the generalized gradient approximation (GGA) was used [27]. For the calculations academic and commercial versions of the *CASTEP* program were employed [28–30]. Ultrasoft pseudopotentials were used with maximum cut-off energy of the plane waves of 380 eV. In addition to the cut-off energy, one further parameter determines the quality of the calculations, namely the density of points with which the Brillouin zone is sampled. Here, a Monkhorst and Pack grid [31] was chosen so that the spacing between the *k*-points was <0.035 $Å^{-1}$. Full geometry optimisations were performed at pressures up to 40 GPa where all structural parameters not fixed by space group symmetry were simultaneously optimized for a given pressure. The remaining stress after the final self-consistency cycle was less than 0.02 GPa, residual forces were less than 0.01 eV/Å. The calculations were performed in the athermal limit, *i.e.*, temperature effects and zero-point motions are neglected.

3. Results and discussion

3.1. High-pressure powder diffraction

The pressure-induced changes in the powder diffraction patterns are shown in Fig. 2. As a representative example, Fig. 3 shows the observed and calculated diffraction patterns resulting from the structure refinement against data collected at 18.3(2) GPa. All reflections were indexed by assigning them to otavite, Ne or Re. The reflection positions of $CdCO_3$ shift continuously with increasing pressure as shown in Fig. 2. It is also seen that the peak profiles of the $CdCO_3$ broaden significantly with the increasing pressure (Fig. 2).

The pressure dependence of the lattice parameters and unit cell volume obtained from the refinements of the powder diffraction data are shown in Fig. 4 in form of normalized lattice parameters a/a_0, c/c_0 and the unit cell volume V/V_0. The compression of $CdCO_3$ is highly anisotropic. In the pressure range up to 10.4(2) GPa the linear compressibility along the *a* axis ($k_a = 0.0010(1)\ GPa^{-1}$) is six times smaller than along the *c*-axis ($k_c = 0.0057(1)\ GPa^{-1}$). In the limit of our experimental resolution there is neither a significant discontinuity in the evolution of the lattice parameters nor in that of the volume (Fig. 4). This indicates that no major change of the compression mechanism occurs up to 40 GPa.

Bulk compressibility data obtained from fits of a third-order Birch–Murnaghan equation-of-state to the unit cell volume are:

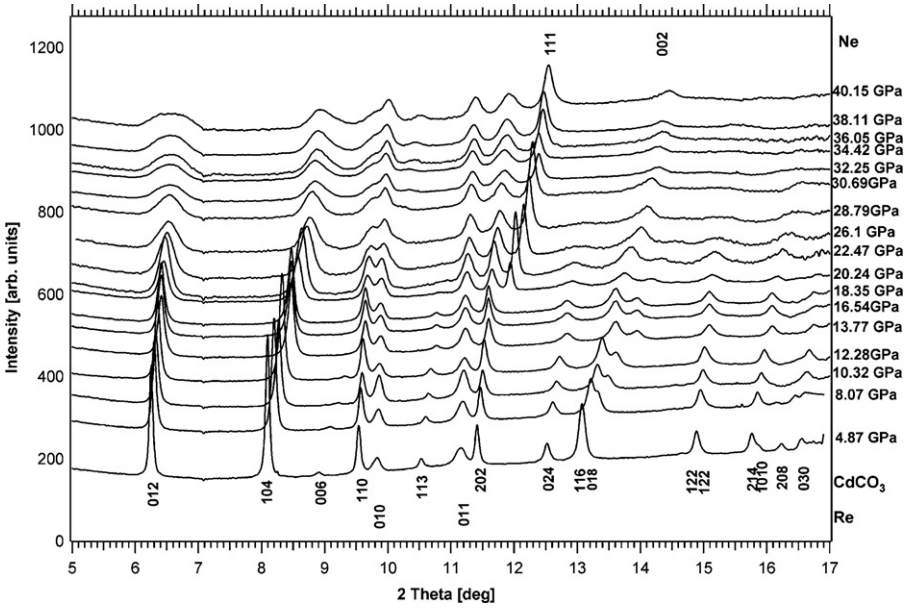

Fig. 2. Pressure dependence of diffraction patterns of $CdCO_3$ from 4.87(5) GPa to 40.2(5) GPa. An arbitrary intensity offset was applied to the diffraction patterns for clarity. Miller indices are given above for the reflections of Ne and below for the $CdCO_3$ and gasket (Re).

$V_0 = 342(1)$ Å^3, $B_0 = 101(3)$ GPa, $B_0' = 2.1(3)$. The small value of the B_0' is well-known for carbonates with a highly anisotropic compression mechanism. For example, for aragonitic $CaCO_3$ [32] and $BaCO_3$ [33], $B_0' = 2.7(7)$ and $B_0' = 1.9(4)$, respectively, were reported.

The changes of lattice parameters with pressure were affected due to changes in the bond lengths and distances, because all atoms in otavite are on special positions (2*b*, 2*a*, 6*f*). Only the oxygen *x*-coordinate may vary. The structure refinements were performed at first with constrained CO_3^{2-} groups to partly compensate the low scattering power of oxygen and carbon compared to cadmium and then repeated without constraints. In both cases, the C–O bonds (1.28(2) Å) and O–C–O angles (120(1)°) remain nearly constant during pressure increase. Therefore, all data shown were obtained with freely refineable oxygen atoms of the CO_3^{2-} - group. The changes of the *x*-coordinate of the oxygen atoms from 0.259(2) at 4.87(5) GPa to 0.26(2) at 40.2(5) GPa are not relevant and are within range of the estimated standard deviation.

The experimentally determined normalized Cd–O bond lengths for all pressures are presented in Fig. 5. Up to 40 GPa Cd–O distances decrease by 9.5(1)% compared to ambient conditions.

3.2. High-pressure Raman spectroscopy

The Raman spectrum of $CdCO_3$ at ambient conditions is well-known [34]. A symmetry analysis showed that five Raman active bands for $CdCO_3$ ($1A_{1g}$ (ν_1), $4E_g$ (ν_3, ν_4, ν_{13}, ν_{14})) are allowed [35]. We observed three bands in the frequency range 150–1800 cm^{-1} assigned to internal vibrations of the CO_3^{2-} group: ν_1 – symmet-

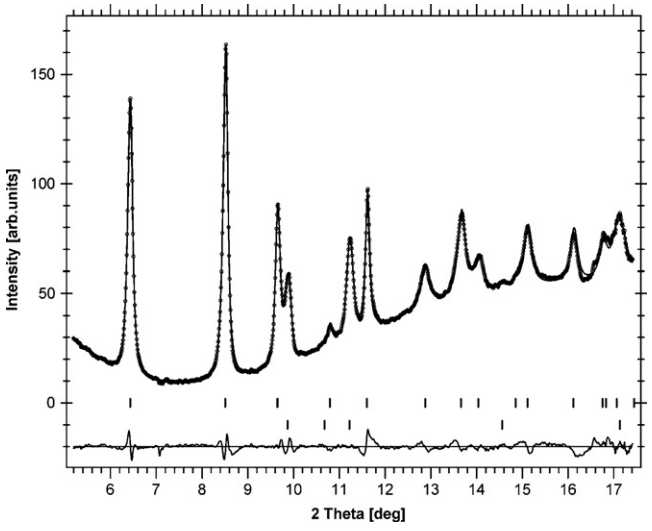

Fig. 3. Rietveld refinement of a powder diffraction pattern of otavite at 18.3(2) GPa. Observed and calculated intensities are shown by the circles and the line, respectively. At the bottom of the figure the difference curve is shown. Tick marks denote reflection positions for $CdCO_3$ (upper row) and Rhenium gasket (lower row).

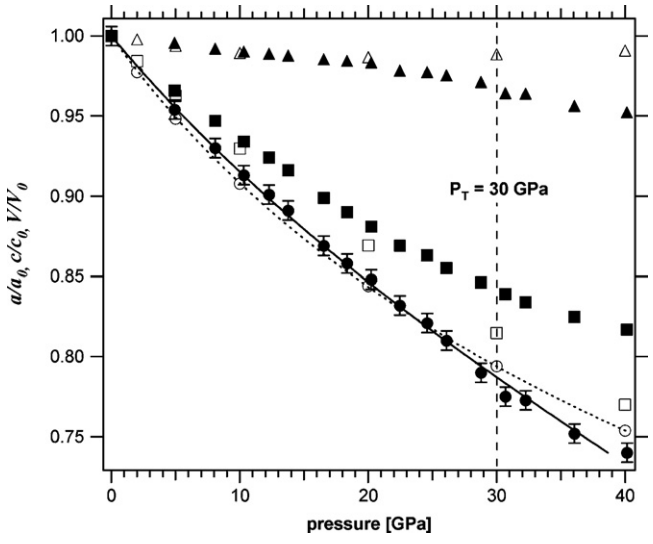

Fig. 4. Evolution of the normalized lattice parameters: a/a_0 (triangles), c/c_0 (squares), and the unit cell volume V/V_0 (circle) with pressure. Open symbols represent data from the *ab initio* calculations, closed symbols show experimental values. If not shown, the error bars for both the pressure and lattice parameters correspond to the size of the symbols. The lines are fits of a third-order Birch–Murnaghan equation-of-state to the experimental (solid line) and obtained by our DFT calculations (dotted line) unit cell volumes.

ric C–O stretching (1088 cm^{-1}); ν_3 – asymmetric C–O stretching (1393 cm^{-1}); ν_4 – in-plane band of the CO_3^{2-} groups (716 cm^{-1}); the first overtone $A_{1g} + E_g$ (1722 cm^{-1}) and two bands assigned to translations and librations of the CO_3^{2-} group relative to the Cd atoms: ν_{13} (275 cm^{-1}), ν_{14} (165 cm^{-1}).

$$S_{ij} = \begin{pmatrix} 0.0089998 & -0.0025598 & -0.0045832 & & & \\ -0.0025598 & 0.0089998 & -0.0045832 & & & \\ -0.0045832 & -0.0045832 & 0.0175520 & & & \\ & & & 0.0327052 & & \\ & & & & 0.0327052 & \\ & & & & & 0.0231191 \end{pmatrix}$$

Raman spectra of $CdCO_3$ as function of pressure up to 23.1(1) GPa are shown in Fig. 6. The behavior of the bands with varying pressure is very similar, namely, with one exception, all bands shift monotonously to higher wave numbers with increasing pressure. The intensity of the ν_{14} band (Fig. 6a), associated with lattice vibration parallel to the *c*-axis, decreases and the band becomes broader. Raman shifts of band positions as function of pressure up to 23.1(1) GPa are shown in Fig. 7. Only for ν_1 – assigned to the symmetric vibration of the CO_3 group, shows a slight change of the slope at approximately 15 GPa. The behavior of all modes is given quantitatively in Table 1. Fig. 8 shows the quantitative evaluation of the full width at the half maximum (FWHM) of the ν_{13} and ν_1 bands with pressure. Significant broadening of the ν_{13} mode, which corresponds to low frequency vibrations, was observed above ~19 GPa. The FWHM is not shown for the ν_{14} band due to the low intensity and strong broadening of this mode with pressure, which made the determination of its exact width difficult.

3.3. Computational results

The evolution of the theoretical obtained lattice parameters and unit cell volume with pressure is presented together with experimental data in Fig. 4. It clearly shows the anisotropic compression behavior of $CdCO_3$. In the pressure range from ambient to 10 GPa the linear compressibility along the *a* axis (k_a = 0.0012 GPa^{-1}) is six times smaller than along the *c*-axis (k_c = 0.007 GPa^{-1}).

The Cd–O bond lengths derived from the *ab initio* calculations are shown in Fig. 5 in combination with experimental data and show only a slight change with pressure. According to the DFT calculations, pressure up to 40 GPa causes shortening of the Cd–O bond by about 7.5% and highly anisotropic compression along the *c*-axis. The bulk volume reduction is 24.6% at 40 GPa. The C–O bond lengths remain constant at about 1.28 Å.

The bulk modulus $B_0 = 1/[3(S_{11} + 2S_{12})]$ = 85.9 GPa was determined from the elastic compliance tensor

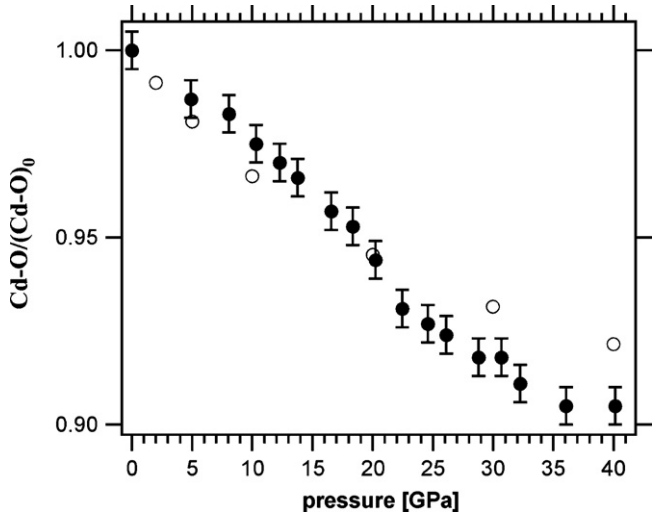

Fig. 5. Comparison of normalized calculated (open symbols) and experimentally obtained (filled symbols) normalized bond lengths Cd–O. The size of the symbols corresponds to errors in pressure.

The fit of a third-order Birch–Murnaghan equation-of-state to the calculated unit cell volumes gives: V_0 = 362.4(1) $Å^3$, B_0 = 89.1(9) GPa, B_0' = 3.39(5).

The pressure dependence of the difference of the molar enthalpies of otavite in the calcite-type structure and for a hypothetic aragonite-type structure is shown in Fig. 9. The negative enthalpy difference ΔH between calcite- and aragonite-type indicates a higher stability of the aragonite structure at high pressures. The pressure of the assumed calcite- to aragonite-type phase transition is ~30 GPa.

3.4. Discussion

The lattice parameters for calcite-type $CdCO_3$ obtained from the *ab initio* calculations are in agreement with experimental data from the literature [3]. The observed differences between both methods are denoted in Table 2. Furthermore, the lattice parameters of aragonite-type $CdCO_3$ and its unit cell volume at ambient conditions [6] are in good agreement with data at the same conditions obtained from our quantum mechanical calculations as well (Table 2).

The comparison of the experimentally and theoretically determined evolution of normalized lattice parameters and volume shows a good agreement up to ~20 GPa (Fig. 4). At higher pressures, significant differences appear with the theoretical model predicting a stronger anisotropy of the compression.

Table 1
Comparison of the *dv/dp* values of $CdCO_3$ modes in the investigated pressure range. Estimated standard deviations of the linear fits are given in parentheses.

Mode	Pressure range (GPa)	*dv/dp* (cm^{-1}/GPa)
ν_{14}	0–23	2.17(8)
ν_{13}	0–23	3.83(2)
ν_3 and ν_4	0–23	1.44(4)
ν_1	0–15	3.12(9)
	15–23	1.54(7)

Table 2
Comparison of lattice parameters of $CdCO_3$ in different structure-types (calcite and aragonite) obtained by different authors and using different methods at ambient conditions.

Borodin et al. [3]	DFT calc., this work	Difference in %
$CdCO_3$ calcite		
a = 4.923(3) Å	*a* = 5.006 Å	1.74
c = 16.287(6) Å	*c* = 16.6274 Å	2.08
V = 341.85(4) $Å^3$	*V* = 362.61 $Å^3$	6.07
Liu and Lin [6]	**DFT calc., this work**	
$CdCO_3$ aragonite		
a = 4.989(3) Å	*a* = 5.151 Å,	3.2
b = 7.822(3) Å	*b* = 7.531 Å	3.84
c = 5.713(4) Å	*c* = 5.893 Å	3.15
V = 222.9(1) $Å^3$	*V* = 228.62 $Å^3$	2.57

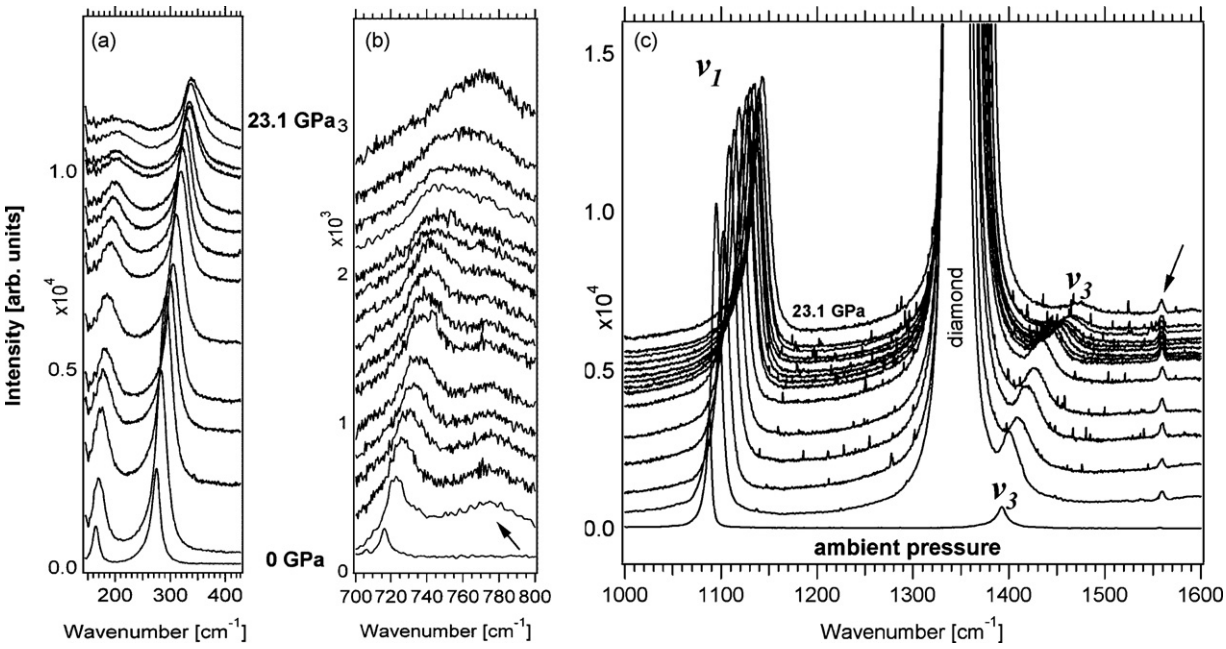

Fig. 6. Raman spectra of $CdCO_3$ as function of pressure in the range 0–23.1(1) GPa: (a) lattice modes ν_{13} (275 cm^{-1}), ν_{14} (165 cm^{-1}), (b) ν_4 – in-plane band of CO_3^{2-} groups, (c) ν_1, ν_3 – symmetric and asymmetric C–O stretching, respectively, diamond signal around 1350 cm^{-1}. The ambient pressure spectrum has been collected without diamond. Arrows denote signals (around 770 cm^{-1} and 1560 cm^{-1}) which appear by using a DAC. Their position does not change with increasing pressure. Spectra are vertically offset for clarity.

The bulk volume reduction in both cases is of the same order of magnitude (24%). The difference in the compression of the Cd–O bonds at 40 GPa between experiment (9.5%) and the calculation (7.8%) is small (Fig. 5). Linear compressibilities, bulk modulus, and V_0 obtained for $CdCO_3$ (calcite-type) in this work and in the earlier published paper [5] are in good agreement (Table 3).

The pressure behavior of $CdCO_3$ is highly anisotropic, with compression along the *c*-axis (Fig. 4) being approximately six times stronger than along the *a*-axis (Table 3). This is related to the shortening of the Cd–O bond lengths (Fig. 5), which was identified as the main structural compression mechanism. The CO_3^{2-} groups remain unchanged during pressure increase in both, experiment and quantum mechanical calculation, and are hence not shown in Fig. 5.

The spectroscopic results are in agreement with the X-ray data. They indicate that the calcite-type structure of $CdCO_3$ is stable up to

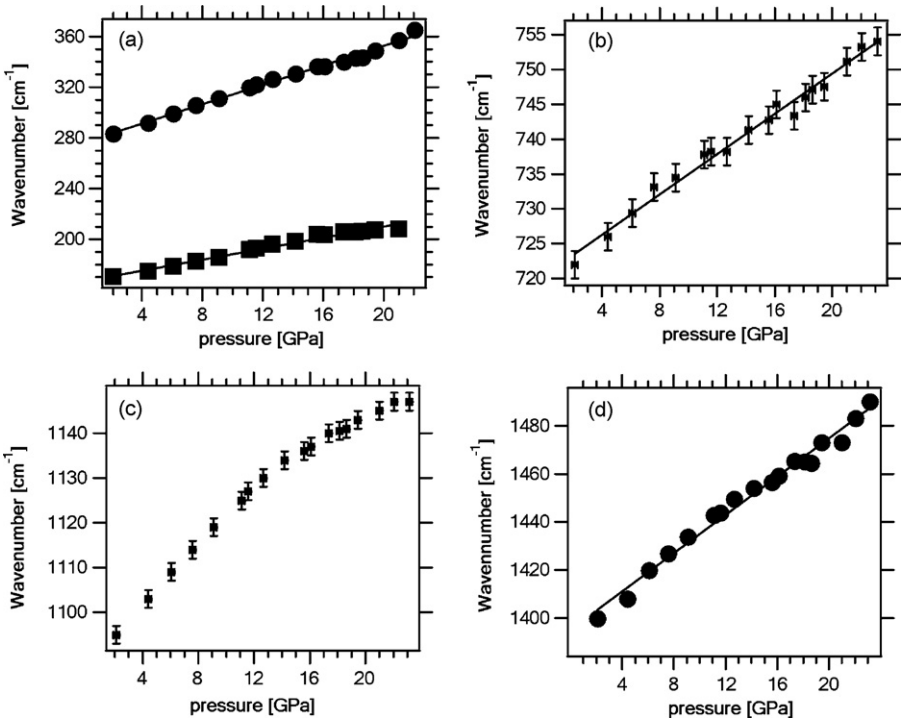

Fig. 7. Pressure-induced mode shifts of $CdCO_3$ on compression: (a) lattice modes: ν_{13} (●), ν_{14} (■); (b) ν_4 – in-plane band of CO_3 group; (c) ν_1 – symmetric vibration of CO_3 group; (d) ν_3 – asymmetric vibrations of the CO_3 group. The size of the symbols corresponds to errors in Raman shift and pressure in figures (a) and (d).

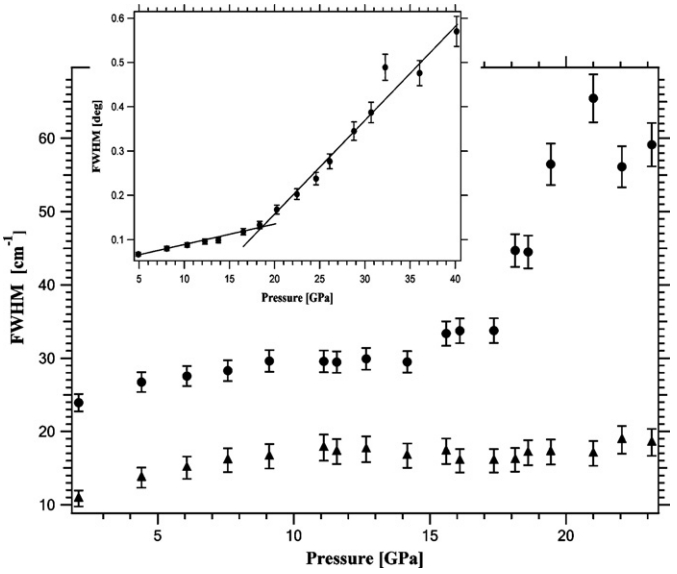

Fig. 8. Evalution of the FWHM of the external ν_{13} (filled circles) and internal ν_1 (filled triangels) Raman modes as function of pressure. The inset highlights the FWHM of the (0 1 2) X-ray reflection as function of pressure. The size of the symbols corresponds to errors in pressure.

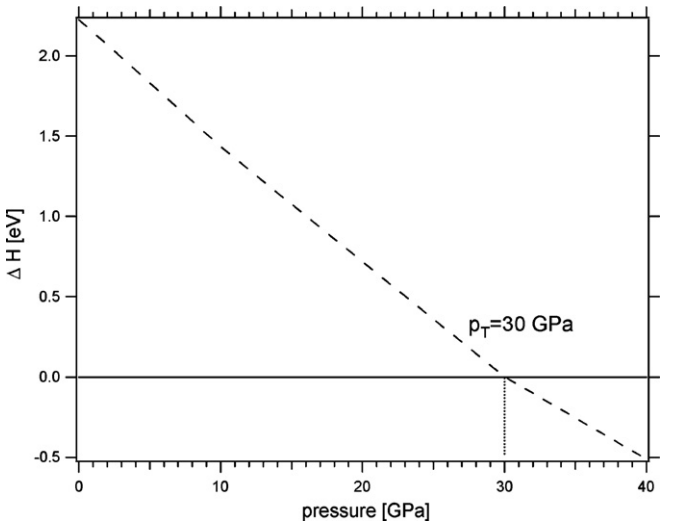

Fig. 9. Pressure dependence of the molar enthalpy difference between calcite and aragonite-type $CdCO_3$ is shown by the dashed line. P_T is the obtained transition pressure.

19 GPa. At pressures exceeding 19 GPa, a strong broadening of the low frequency Raman bands (ν_{13}, ν_{14}) and of the X-ray diffraction peaks is observed (Figs. 2, 6a and 8). Interestingly, the *ab initio* calculations predict a calcite–aragonite-type transition at a pressure of p_T = 30 GPa (Fig. 9). The quantitative evaluation of the FWHM of Raman modes (ν_{13}, ν_1) and, exemplary, of the diffraction peak (0 1 2) (Fig. 8, inset) are presented in Fig. 8. While the FWHM of the $CdCO_3$ X-ray diffraction peak and ν_{13} Raman bands show a broadening above about 19 GPa with increasing pressure, the ν_1 mode, which is associated with symmetric C–O stretching in the CO_3 groups, remains sharp. Possible explanations for these findings are:

(i) A possible calcite-type to aragonite-type transition or a transition to an unknown high-pressure phase in $CdCO_3$ would lead to broadening or splitting of external Raman bands (ν_{13}, ν_{14}) and X-ray reflections. The observed broadening of the latter may be related to insufficient resolution of the X-ray experiment preventing a clear detection of a possible splitting of reflexions (Figs. 2 and 8 inset). The broadening of the low frequency Raman modes (Fig. 8) suggests changes in the long range order of the structure. This may be seen as equivalent to a symmetry change that supports our proposal of a phase transition. Because a calcite-type to aragonite-type transition in carbonates does not affect the symmetry of the CO_3 groups, the FWHM of the ν_1 mode remains almost constant (Fig. 8).

(ii) An alternative explanation for the peak broadening would be the existence of non-hydrostatic conditions in the sample chamber. It is well-known that in high-pressure experiments such conditions may be responsible for asymmetric peak shapes, splitting, and/or broadening of diffraction lines [36]. Furthermore, the equation-of-state may be biased by non-hydrostatic stresses. Non-hydrostatic stresses may either promote [37], or suppress [38] phase transformation or even cause the sample to become amorphous [39].

Unfortunately, it is very difficult to quantify the stress state of a non-hydrostatic pressure medium. It should be noted, however, that the high-pressure behavior of Neon as a pressure transmitting medium is very well-known [40–44]. Recently, Klotz et al. [45] estimated that, while the first signs of non-hydrostaticity of Ne may appear at 15 GPa, pressure gradients are less than 0.2 GPa at 30 GPa and 0.3 GPa at 40 GPa. Consequently, Ne may be considered to be at least quasi-hydrostatic at all conditions of our experiments, and thus with only little influence on the obtained spectra and diffraction patterns.

In general, non-hydrostatic conditions should affect all compounds in the sample chamber similarly. However, only strong broadening of $CdCO_3$ X-ray reflections is observed, whereas the Neon peaks remain sharp (Fig. 2). In the Raman measurements only the external modes are affected, while the internal ν_1 band remains sharp (Figs. 6 and 8). Therefore, the observed broadening is considered inherent to $CdCO_3$ and only negligibly related to the experimental conditions.

Of course, it cannot be excluded that the peak profiles are simultaneously affected by both effects, a phase transition and non-hydrostaticity. Nonetheless, we are in favour of relating the observed broadening of signals in our experiments to a phase transition in $CdCO_3$.

It is worth mentioning that our diffraction data collected above 19 GPa cannot be fitted with the aragonitic cell parameters for $CdCO_3$ as suggested by Lin and Liu [6]. Also, diffraction patterns collected above 30 GPa cannot be fitted with the aragonite-type structure model obtained in our quantum mechanical calculations for 30 GPa. The modelled aragonite diffraction pattern for $CdCO_3$ at 30 GPa has a very strong reflection (-1 1 1) at the $2\theta = 7.18^\circ$, which definitely does not exist in our measured X-ray data (Fig. 2). This may suggest an even more complicated p_T phase diagram for $CdCO_3$. It was recently found for aragonite-type carbonates [12,16,46] that their phase diagrams are more complex than assumed. Also, it could support the theory that no calcite- aragonite phase transitions for carbonates with *d* transition metal cations exist in the investigated pressure range.

Table 3
Comparison of linear compressibilities, bulk moduli and V_0 for $CdCO_3$ (calcite).

Zhang and Reeder [5]	X-ray, this work	DFT calc., this work
$V_0 = 342.50(5)$ Å^3	$V_0 = 342(1)$ Å^3	$V_0 = 362.4(1)$ Å^3
$B_0 = 97(1)$ GPa	$B_0 = 101(3)$ GPa	$B_0 = 89.1(9)$ GPa
	$B' = 2.1(3)$	$B' = 3.39(5)$
$k_a = 0.00128(4)$ GPa^{-1},	$k_a = 0.0010(1)$ GPa^{-1},	$k_a = 0.0012$ GPa^{-1}
$k_c = 0.00651(9)$ GPa^{-1}.	$k_c = 0.0057(1)$ GPa^{-1}.	$k_c = 0.007$ GPa^{-1}

4. Conclusions

The stability of $CdCO_3$ up to 19 GPa and the change in the behavior of external modes above 19 GPa, that proposes the change of the symmetry, were determined using Raman spectroscopy. The elastic behavior of $CdCO_3$ was investigated up to 40 GPa using X-ray diffraction. Bulk moduli and linear compressibilities were determined experimentally and compared with results from DFT calculations. The values obtained by both methods show good agreement with literature [6].

In contrast to our DFT calculations, which suggest a calcite–aragonite-type phase transition in $CdCO_3$ at 30 GPa, our experimental data propose a phase transition to occur at a lower pressure in unknown structure. Thus, the consistent broadening of the FWHM of the low frequency Raman mode (ν_{13}) and the diffraction peaks suggests that a phase transition occurs in $CdCO_3$ at or above ~19 GPa (Fig. 8). However, it is not a calcite–aragonite-type phase transition in $CdCO_3$.

Despite having almost the same size of the cation, $CdCO_3$ and $CaCO_3$ seem to behave substantially differently at high pressures. The considerably higher pressure stability of otavite with respect to calcite, where the calcite to $CaCO_3$-II transformation occurs at 1.5 GPa [47], can be attributed only to the significantly different electron configuration of Cd^{2+} and Ca^{2+}. Hence, we conclude that the pressure homologue rule does not necessarily hold for cations with different valence spheres (*s* vs. *d* orbitals).

Further *in-situ* p_T experiments with improved resolution are needed to unambiguously elucidate the structural behavior of otavite at extreme conditions.

Acknowledgements

This research was supported by the Deutsche Forschungsgemeinschaft under project number KN 507/5-1 in the framework of the priority program: "Synthesis, '*in situ*' characterization and quantum mechanical modelling of Earth Materials, oxides, carbides, and nitrides at extremely high pressures and temperatures". The use of the beamline X17C was supported by COMPRES, the Consortium for Materials Properties Research in Earth Sciences under NSF Cooperative Agreement EAR 06-49658. Use of the National Synchrotron Light Source, Brookhaven National Laboratory, was supported by the U.S. Department of Energy, Office of Science, Office of Basic Energy Sciences, under Contract No. DE-AC02-98CH10886. The authors would like to thank C. Tarabrella, Q. Guo and J. Hu for help during the measurements. Y. Lee and D.H. Seoung thank the support from the BK21 program to the Institute of Earth, Atmosphere, and Astronomy at Yonsei University and the Global Research Lab Program of the Ministry of Education, Science and Technology (MEST) of the Korean Government. Bjoern Winkler is grateful for funding from the BMBF in the framework of the Geotechnologienprogramm 03G0717B.

References

[1] D.L. Graf, Am. Mineral. 46 (1961) 1283–1316.
[2] R.E. Kirk, D.F. Othmer, A. Seidel, Vol. 2, 5 ed., Wiley-Interscience, Hoboken, NJ, 2007.
[3] V.L. Borodin, V.I. Lyutin, V.V. Ilyukhin, N.V. Belov, Doklady Akademii Nauk SSSR 245 (1979) 1099–1101.
[4] R.D. Shannon, Acta Crystallogr. A 32 (1976) 751–767.
[5] J.Z. Zhang, R.J. Reeder, Am. Mineral. 84 (1999) 861–870.
[6] L.G. Liu, C.C. Lin, Am. Mineral. 82 (1997) 643–646.
[7] G.M. Brown, Vol. McGraw-Hill, New York, 1975.
[8] J. Santillan, Q. Williams, Phys. Earth Planet. Inter. 143–144 (2004) 291–304.
[9] S. Ono, Mineral. Mag. 71 (2007) 105–111.
[10] S.M. Antao, I. Hassan, Phys. Chem. Miner. 34 (2007) 573–580.
[11] F. E. Brenker, C. Vollmer, Vincze L., Vekemans B., Szymanski A., Janssens K., Szaloki I., Nasdala L., Joswig W., K. F., Earth Planet. Sci. Lett. 260 (2007) 1–s9.
[12] S. Ono, Phys. Chem. Miner. 34 (2007) 215–221.
[13] S. Ono, T. Kikegawa, Y. Ohishi, Am. Mineral. 92 (2007) 1246–1249.
[14] A.R. Oganov, S. Ono, Y.M. Ma, C.W. Glass, A. Garcia, Earth Planet. Sci. Lett. 273 (2008) 38–47.
[15] R. Minch, L. Dubrovinsky, A. Kurnosov, L. Ehm, K. Knorr, W. Depmeier, Phys. Chem. Miner. 37 (2010) 45–56.
[16] R. Minch, L. Peters, L. Ehm, K. Knorr, O. Siidra, V. Prakapenka, P. Dera, W. Depmeier, Z. Kristallogr. 225 (2010) 146–152.
[17] H. Mao, P. Bell, J. Shaner, D. Steinberg, J. Appl. Phys. 49 (1978) 3276–3283.
[18] A.P. Jephcoat, L.W. Finger, D.E. Cox, High Press. Res. 8 (1992) 667–676.
[19] A. Hammersley, S. Svensson, M. Hanfland, A. Fitch, D. Häusermann, High Press. Res. 14 (1996) 235.
[20] H. Rietveld, Acta Crystallogr. 22 (1967) 151–152.
[21] A.A. Coelho, TOPAS: General profile and structure analysis software for powder diffraction data, 2000.
[22] P. Thompson, D.E. Cox, J.B. Hastings, J. Appl. Crystallogr. 20 (1987) 79–83.
[23] W. Dollase, J. Appl. Crystallogr. 19 (1986) 267–272.
[24] J.-F. Berar, P. Lelann, J. Appl. Crystallogr. 24 (1991) 1–5.
[25] F. Birch, J. Geophys. Res. 83 (1978) 1257–1268.
[26] D.R. Allan, R. Miletich, R.J. Angel, Rev. Sci. Instrum. 67 (1996) 840–842.
[27] J.P. Perdew, K. Burke, M. Ernzerhof, Phys. Rev. Lett. 77 (1996) 3865–3868.
[28] V. Milman, B. Winkler, J.A. White, C.J. Pickard, M.C. Payne, E.V. Akhmatskaya, R.H. No-bes, Int. J. Quantum Chem. 77 (2000).
[29] S.J. Clark, M.D. Segall, C.J. Pickard, P.J. Hasnip, M.I.J. Probert, K. Refson, M.C. Payne, Z. Kristallogr. 220 (2005) 567–570.
[30] M.D. Segall, P.J.D. Lindan, M.J. Probert, C.J. Pickard, P.J. Hasnip, S.J. Clark, M.C. Payne, J. Phys. Condens. Matter 14 (2002) 2717–2744.
[31] H.J. Monkhorst, J.D. Pack, Phys. Rev. B 13 (1976) 5188–5192.
[32] I. Martinez, J. Zhang, R.J. Reeder, Am. Mineral. 81 (1996) 611–624.
[33] C.M. Holl, J.R. Smyth, H.M.S. Laustsen, S.D. Jacobsen, R.T. Downs, Phys. Chem. Miner. 27 (2000) 467–473.
[34] H.N. Rutt, J.H. Nicola, J. Phys. C: Solid State Phys. 7 (1974) 4522–4528.
[35] W.B. White, in The Infrared Spectra of Minerals. (Ed.: V.C. Farmer), Mineralogical Society Monograph, London, 1974, pp. 227–279.
[36] N. Funamori, M. Funamori, R. Jeanloz, N. Hamaya, J. Appl. Phys. 82 (1997) 142–146.
[37] R. Resel, M. Oezelt, K. Shimizu, A. Nakayama, K. Takemura, Solid State Commun. 129 (2004) 103–106.
[38] D.L. Decker, S. Petersen, D. Debray, Phys. Rev. B (1979) 3552–3555.
[39] V. Dmitriev, V. Sinitsyn, R. Dilanian, D. Machon, A. Kuznetsov, E. Ponyatovsky, G. Luca-zeau, H.P. Weber, J. Phys. Chem. Solids 64 (2003) 307–312.
[40] R.J. Angel, M. Bujak, J. Zhao, G.D. Gatta, S.D. Jacobsen, J. Appl. Crystallogr. 40 (2007) 26–32.
[41] L.W. Finger, R.M. Hazen, G. Zou, H.K. Mao, P.M. Bell, Appl. Phys. Lett. 39 (1981) 892–894.
[42] R.J. Hemley, C.S. Zha, A.P. Jephcoat, H.K. Mao, L.W. Finger, Phys. Rev. B 39 (1989) 11820–11827.
[43] W.L. Vos, J.A. Schouten, D.A. Young, M. Ross, J. Chem. Phys. 94 (1991) 3538–3838.
[44] A. Dewaele, F. Datchi, P. Loubeyre, M. Mezouar, Phys. Rev. B 77 (2008).
[45] S. Klotz, J.C. Chervin, P. Munsch, G. Le Marchand, J. Phys. D-Appl. Phys. 42 (2009) 1–7.
[46] S. Ono, M. Shirasaka, T. Kikegawa, Y. Ohishi, Phys. Chem. Miner. 32 (2005) 8–12.
[47] L. Merrill, W.A. Bassett, Acta Crystallogr. B 31 (1975) 343–349.